

# Design and Preliminary Characterization of the USNO Rubidium Fountain

Steven Peil, Scott Crane, Thomas B. Swanson, and Christopher R. Ekstrom

Time Service Department, Clock Development Division

U. S. Naval Observatory

Washington, D. C.

**Abstract**—We have built and begun characterization of an engineering prototype rubidium atomic fountain at the USNO for use in its clock ensemble. We achieve short-term stability of  $1.4 \times 10^{-13}/\tau^{1/2}$ , which meets the desired performance for characterizing maser drift. We will discuss the design, operation, and preliminary characterization of this device.

## I. INTRODUCTION

The United States Naval Observatory's Master Clock utilizes more than five dozen atomic clocks to, typically contributing on order of 40% of the weight of TAI. Currently, active hydrogen masers provide the high short-term stability, and maser drift is steered out using commercial cesium-beam clocks. In order to meet future demands, the Observatory plans to use several rubidium atomic fountain clocks to characterize masers and detect changes in maser performance more rapidly. This will improve both the stability and robustness of the timescales.

For this purpose, these systems need to perform in an operational environment without user intervention. We have built a prototype device consisting of three equipment racks plus a Ti:sapphire laser (a rack-mounted laser, based on fiber amplification and frequency doubling of a 1560 nm source, is under development). Microwave synthesis and all of the optical-beam splitting and modulation are carried out in rack-mounted shelves [1]. Laser-frequency and power servos are among the user-configurable electronics modules that we designed. Data acquisition and timing are executed with compact PCI (PXI) instrumentation. One of the three equipment racks is the ‘physics package’, with a footprint of 0.8 m × 0.8 m.

## II. PHYSICS PACKAGE

A cutaway of the fountain apparatus is shown in Fig. 1. The physics package is entirely enclosed in a magnetic shield set, with three layers of shielding for the atom collection/launching, state preparation, and detection regions. A fourth magnetic shield encloses the microwave spectroscopy and free-precession regions.

A 1 mG bias magnetic field (the “C-field”) for the spectroscopy and free-precession regions is produced by a current of 100 μA through a two-layer solenoid. Coils consisting of several turns provide shimming of the C-field near the end of the solenoid to increase the field uniformity. Following fields to ensure adiabatic transport between the state-selection cavity and the free-precession region are created by several ~4 turn coils.

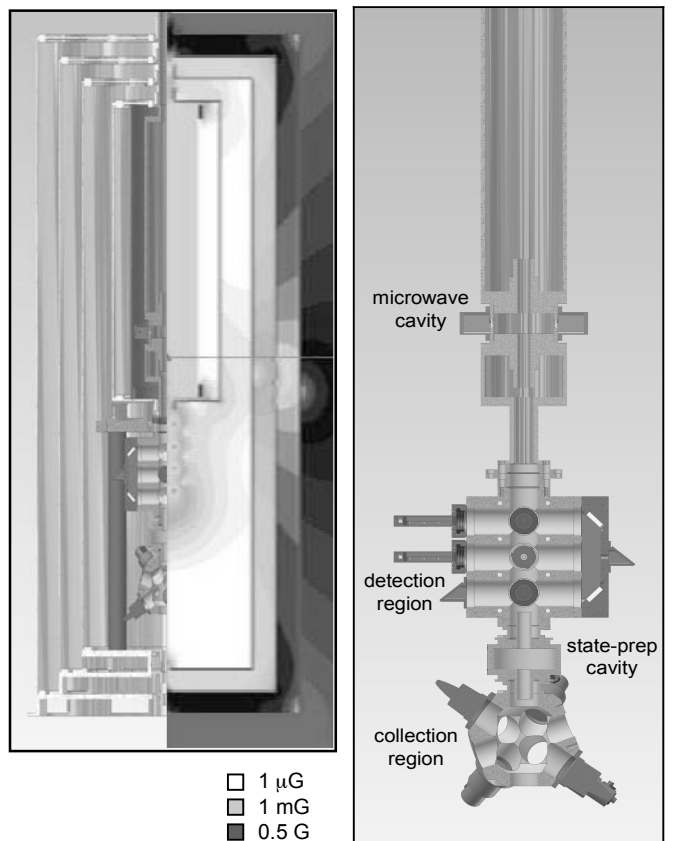


Figure 1. Left: Cross section of physics package along with calculated magnetic field map. Right: Close up of the cross sectional view of the vacuum chamber and optical couplers.

The magnetic shielding produces a zero-field region for optimal molasses cooling and for generation of the small, controlled bias fields elsewhere. Everything within the shields must, therefore, be “nonmagnetic” in construction, having both low permeability and small permanent magnetic moments. All vacuum chamber components are either titanium (CP Grade II and IV) or OFHC copper, and are assembled with titanium conflat flanges or e-beam welded joints. Supporting structure materials are either titanium or aluminum.

There are two sections of the vacuum chamber that require optical access, the collection chamber and the detection chamber. These two vacuum parts are machined from titanium with weld preps for weld-in windows. The weld-in windows are sapphire flats brazed to a thin titanium collar and have a 36 mm clear aperture [2]. The small size of these window assemblies allows for compact chambers and excellent optical access.

The microwave interrogation cavity is made of OFHC copper, has a Q of 6,500 and an axial aperture for the atoms that is 18 mm in diameter. All of the vacuum chamber inside the inner shield is OFHC copper as well. This requires a transition to titanium to make conflat seals. This transition is made with a Cu-Ti explosion-bonded flange that is e-beam welded to the copper chamber. The state selection microwave cavity is made out of titanium. Both cavities have two microwave feeds at their equators with alumina windows for coupling the microwaves through the vacuum envelope. Heaters for tuning the spectroscopy cavity to resonance and for temperature regulation are driven with AC currents, chosen at audio frequencies far from any atomic resonance or experimentally sensitive values.

All laser light used for cooling/launching, state preparation, and detection are delivered via polarization maintaining (PM) or polarizing (PZ) optical fiber from the rack-mounted optical tables to the physics package. Beam shaping is done with fiber-coupled monolithic lens assemblies to produce both the collection/launching beams and the detection light sheets. Small coils carrying a current of 2.5 A provide a modest field gradient (2 G/cm axially) for MOT collection. We can choose not to use this field and instead load directly into a  $\sigma^+ - \sigma^-$  molasses. The six laser beams for collecting atoms from the background vapor are ~23 mm in diameter<sup>1</sup> and are oriented to launch the atoms vertically in the <1,1,1> direction. We currently operate with 15-20 mW of power in each beam.

We use one light sheet with a 15 mm × 2.5 mm cross section for detection of atoms in each state by scattering light from atoms in the F=2 state. This traveling wave also removes atoms in the F=2 state from the fountain trajectory as part of the state selection process. A second light sheet, situated between the two fluorescence collection regions, (re)pumps the atoms from F=1 to F=2. After (re)pumping, the atoms detected in the second pass through the light sheet

represent the atoms initially in the F=1 state. Light scattered by the atoms during detection is collected with an assembly of two aspheric F/0.64 lenses, 38 mm in diameter, that image the atomic fluorescence onto a 1 cm × 1 cm photodiode with an integrated transimpedance amplifier. Light scattered in the opposite direction of the detector is reflected back toward the collection optics with a spherical mirror. All light intensities are stabilized; we use large-core (400  $\mu\text{m}$ ) multimode fibers to collect a sample of the beam and guide it to a photodiode located in an electronics rack. In this way electrical pickup from heaters and ground loops can be minimized.

### III. OPERATION

A fountain cycle is 1.2 s long and consists of several stages. Rubidium 87 atoms are loaded for 300 ms into either a MOT ( $\sim 10^8$  atoms) or an optical molasses ( $\sim 5 \times 10^6$  atoms), with a laser detuning of  $\sim 3\gamma$  (17MHz/6MHz). In the former case, the MOT currents are turned off, and after a 40 ms delay for the field to decay, atoms are cooled for 10 ms with molasses.<sup>2</sup> The detuning of the upward-directed beams is switched to be 3.1 MHz below that of the downward-directed beams to accelerate the atoms, which attain a velocity of 4 m/s within 800  $\mu\text{s}$ . A second stage of molasses cooling is carried out in the reference frame of the moving atoms for 1.6 ms by detuning the beams to  $8\gamma$  (47MHz/6MHz) and adiabatically reducing the launch beam intensity to zero power in 200  $\mu\text{s}$ . This results in a cloud of atoms with temperature (from the FWHM of the time-of-flight signals) of  $\sim 1.5 \mu\text{K}$ .

The presence of repump light during the launch phase ensures that all of the atoms end up in the F=2 state, and a mixture of  $m_F$  states, by the time they leave the collection region. As they cross the state-preparation cavity, atoms in the  $|F=2, m_F=0\rangle$  state are driven to  $|1, 0\rangle$  via a resonant microwave  $\pi$  pulse. Atoms in the  $|2, m_F\neq 0\rangle$  states are removed from the fountain trajectory with resonant light scattering by the probe beam. The  $|1, 0\rangle$  atoms undergo Ramsey interrogation and the atoms’ final state is read out in the detection region. With our fountain geometry and atom temperature, ~20% of the atoms should make it back through the aperture in the microwave cavity and be available for detection. We measure a return fraction of about 5%, which is consistent with calculations that indicate the additional loss is due to collisions with background rubidium atoms from the higher-pressure collection chamber.

The central Ramsey fringe is interrogated by phase modulating our microwave chain. Alternate fountain cycles advance or retard the phase of the microwaves in the spectroscopy cavity by 90 degrees. This phase modulation is provided by a direct digital synthesizer. The transition

---

<sup>1</sup> All beam dimensions are quoted as twice the beam waist.

<sup>2</sup> The 40 ms required for the MOT field to decay is the same whether the three outermost magnetic shields are on or off. This may allow us to run with the weak-field MOT inside the shields.

probability for a given fountain cycle is compared to the transition probability from the previous cycle (along with the direction of the phase changes for the two cycles) to calculate the difference between the local oscillator and the fountain frequencies. This method of estimating the frequency differences between the fountain and its local oscillator produces a time series that will give an artificially low estimation of the Allan Deviation at one cycle time,  $\tau = \tau_0$ , so all stability plots suppress this point and start at  $\tau = 2\tau_0$ .

#### IV. PERFORMANCE

The stability data presented here were all taken using a MOT to collect atoms. We currently measure roughly 3 times worse short-term stability when loading with an optical molasses. We are working to both increase the optical molasses loading and studying MOT operation within the magnetic shields.

The local oscillator for our frequency chain is a high stability, low phase noise crystal oscillator. This crystal can be locked to an external frequency reference with a phase locked loop (PLL) with a time constant of 1-10 seconds. Fig. 2 shows the performance of the fountain when running against the free-running crystal oscillator. The stability is better than  $10^{-13}$  for times less than 100 s. The performance of this crystal opens up the possibility of directly steering this local oscillator.

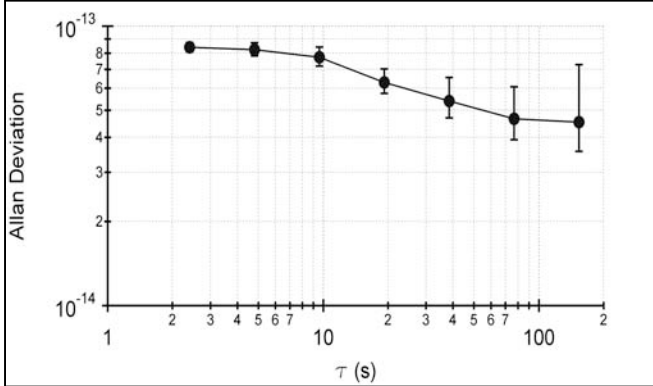


Figure 2. Fountain stability when referenced to a free-running crystal.

We have also run the fountain with the crystal oscillator phase locked to several different active hydrogen masers. Fig. 3 shows the stability of the fountain with the crystal locked to a maser with good short-term stability and close-to-carrier phase noise. The phase locked loop's time constant was roughly 4 seconds. The short-term performance is consistent with white frequency noise and a stability of  $1.4 \times 10^{-13}/\tau^{1/2}$ . An optimized PLL tuning for this combination of maser and crystal may allow for improved short-term stability.

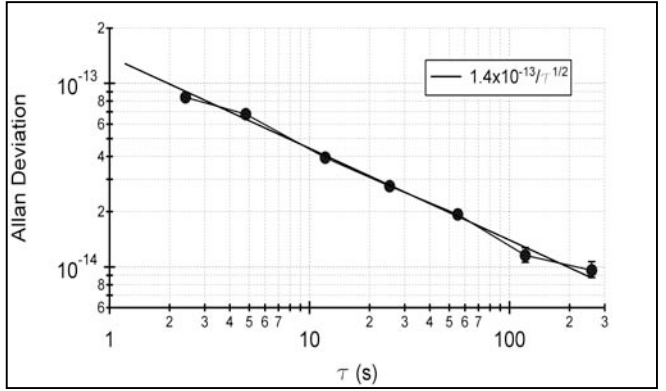


Figure 3. Short-term stability when the crystal is phase-locked to a hydrogen maser.

Fig. 4 shows the stability of a longer run of the fountain. For this data set, the local oscillator was our crystal locked to a maser (different from that used to produce the data in Fig. 3). The short-term stability is  $2 \times 10^{-13}/\tau^{1/2}$  with deviations from white frequency behavior after about 2,000 seconds. The excess noise at averaging times over 2,000 seconds is consistent with the operation of the reference maser as measured in the USNO ensemble. We are not able to say with confidence that the stability of the fountain continues to improve after an averaging time of  $10^5$  seconds. We have tried to estimate the fountain's stability at longer times with three-cornered-hat techniques. These comparisons were performed by steering the output of the reference maser and measuring the steered output in one of the USNO clock ensemble measurement systems. While some of these estimates seem to indicate that the fountain continues to exhibit white frequency noise at longer averaging intervals, the confidence intervals on these estimates are large and indicate the need for longer comparisons.

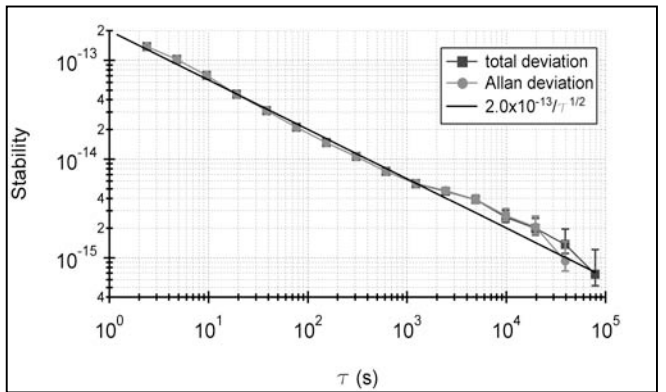


Figure 4. Longer averaging times of the fountain versus maser performance.

Longer evaluations have been hampered by the length of time over which the Ti:sapphire laser remains locked to the correct reference-cavity mode and also remains free from contamination. We expect to be able to run continuously once the development of our frequency-doubled laser is complete. We have been able to use a version of this laser to

run the fountain with short-term performance degraded by a factor of  $\sim 3\text{-}4$ .

In addition to implementing our new laser system, maintenance to our cesium fountain [3] should provide us with a second clock of comparable performance, allowing us to determine medium- and long-term performance of the rubidium system in a much more straightforward way.

## V. CONCLUSIONS

In conclusion, we have built and begun characterization of an engineering prototype rubidium atomic fountain at the USNO for use in its clock ensemble. We achieve short-term stability of  $1.4 \times 10^{-13}/\tau^{1/2}$ . We have demonstrated

uninterrupted runs of several days and implemented a steered output for our ensemble measurement systems.

## REFERENCES

- [1] S. Crane, S. Peil, and C. R. Ekstrom, "Miniaturized Atomic Fountain Optical Table," Proceedings of the IEEE International Frequency Control Symposium, 2005.
- [2] S. Crane and C. R. Ekstrom, "Nonmagnetic UHV Optical Viewports," Proceedings of the IEEE International Frequency Control Symposium, 2005.
- [3] C. R. Ekstrom, E. A. Burt, and T. B. Swanson, "Characterization of the USNO Cesium Fountain," Proceedings of the IEEE Frequency Control Symposium, 2001, pp. 53–56.